Journal of Hydrology 593 (2021) 125916

Contents lists available at ScienceDirect

Journal of Hydrology

journal homepage: www.elsevier.com/locate/jhydrol

Research papers

On the thermodynamic foundations of the complementary relationship of evaporation

Jozsef Szilagyi [a,b,*]

[a] Department of Hydraulic and Water Resources Engineering, Budapest University of Technology and Economics, H-1111 Muegyetem Rkp. 1-3, Budapest, Hungary
[b] Conservation and Survey Division, School of Natural Resources, University of Nebraska-Lincoln, Lincoln, Nebraska, USA

ARTICLE INFO

This manuscript was handled by Marco Borga, Editor-in-Chief, with the assistance of Yuting Yang, Associate Editor

Keywords:
Complementary relationship
Land evaporation
Water phase-diagram
Isenthalps

ABSTRACT

The simultaneous thermodynamic pathways (i.e., isenthalps) of the air at the measurement height and at the vegetated land surface under isobaric and adiabatic wetting/drying cycles of the environment make it possible to define the actual evaporation rate with the help of three (one measured and two derived) vapor pressure (and corresponding temperature) terms. From the first-order approximation about the constancy of the relative average speed which the two isenthalps are travelled at during drying out of the environment, a non-dimensional, linear form of the complementary relationship (CR) of evaporation naturally emerges, but now expressed by vapor pressures (and temperatures, respectively). Without an artificially low Priestley-Taylor parameter value this linear CR would overestimate the evaporation rates because the surface warms faster than the constant relative speed assumption permits. With the appropriate estimation of the wet-surface temperature and employment of realistic boundary conditions, the latter leading to a nonlinear CR, land evaporation rates can be estimated fairly accurately with minimal input variables (air temperature, humidity, wind speed and net surface radiation) and without any information of land surface properties. Not only actual but three potential evaporation rates can also be defined by linking the temperature/vapor pressure coordinates of the air and the surface isenthalps, thus reproducing certain existing formulations of the CR as well as re-creating an existing hybrid (containing, both non-dimensional vapor pressure and evaporation terms) version of it.

1. Introduction

The complementary relationship (CR) of evaporation, first proposed by Bouchet (1963), is one of the few tools available to hydrologists, civil/biological/environmental engineers, hydro-meteorologists, and climate modelers to estimate actual land evaporation rates with minimal (atmospheric and radiation) input data requirements and without detailed knowledge of the land-surface properties. While the CR is widely accepted to build on the intricate feedback mechanism present in the land–atmosphere interface (Brutsaert, 1982; Morton, 1983), its critiques see it as merely an heuristic approach, without much concrete physical basis (McNaughton and Spriggs, 1989) or valid only under certain environmental conditions (Shuttleworth et al., 2009), potentially contributing to its largely underemployed and overlooked status in the hydrological, hydro-meteorological, and climate modeling community, despite numerous highly successful efforts to prove the predictive power of its recently developed non-dimensional versions (Brutsaert, 2015; Crago et al., 2016; Brutsaert et al., 2017, 2020; Han and Tian, 2018). A calibration-free, non-dimensional, and nonlinear version of the CR (Szilagyi et al., 2017) has also been systematically compared to other, more data intensive and complex −remote-sensing, reanalysis, land surface model, and machine-learning based−methods on a continental scale for further demonstration of its capabilities (Szilagyi, 2018; Ma et al., 2019; Ma and Szilagyi, 2019, Ma et al., 2020; Szilagyi et al., 2020). Despite of its remarkable performance, the CR still needs a long overdue clear, physically based derivation for an anticipated better acceptance and wider recognition by the geophysical community in large.

The CR has classically been based on the realization that the actual unknown land evaporation rate, E (m s^{-1}) can be inferred from evaporation rates of two wet land surfaces different only in spatial extent: one is plot-sized (with corresponding evaporation rate of E_p), the other regionally significant (with evaporation rate of E_w). The difference in the two wet-surface evaporation rates ($E_p \geq E_w \geq E$) is caused by horizontal

* Corresponding author at: Department of Hydraulic and Water Resources Engineering, Budapest University of Technology and Economics, H-1111 Muegyetem Rkp. 1-3, Budapest, Hungary.
E-mail address: szilagyi.jozsef@epito.bme.hu.

https://doi.org/10.1016/j.jhydrol.2020.125916
Received 9 September 2020; Received in revised form 19 November 2020; Accepted 16 December 2020
Available online 5 January 2021

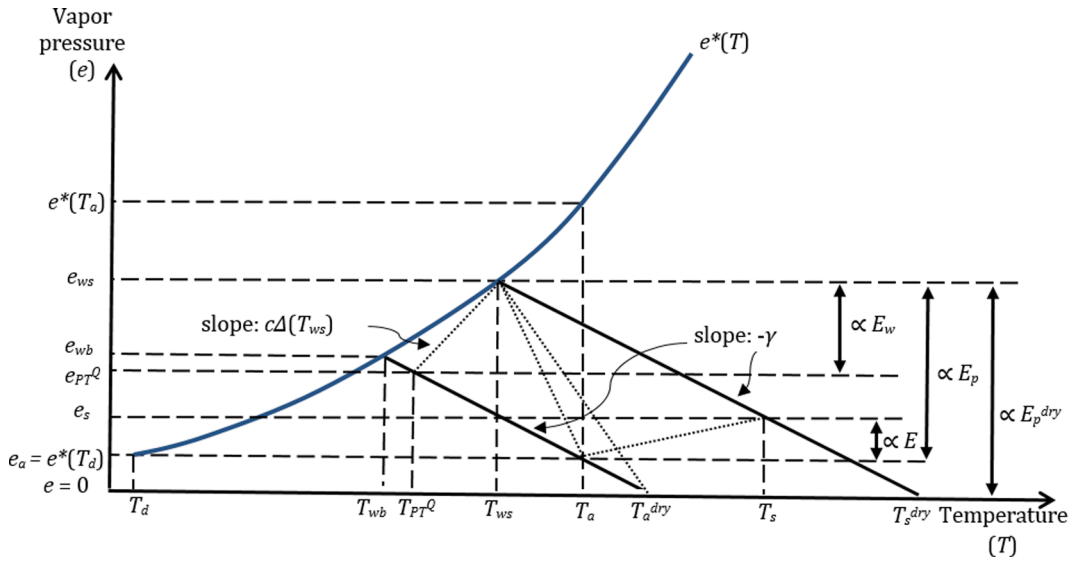

Fig. 1. Schematics of the saturation vapor pressure (e^*) curve, the air (bottom) and vegetated land surface (top) isenthalps of slope -γ, as well as the tangent line (Δ) of e^* at the wet surface (T_{ws}) temperature multiplied by a constant, c (>1). The vertical projections of the four dotted lines are proportional ($\propto$) to the different evaporation rates specified, while the horizontal projections to the sensible heat, this latter being negative with E_p and E_p^{dry}. See Table 1 for the definition of evaporation rates and the relevant temperatures.

energy advection (called 'oasis effect') which becomes stronger with the drying of the environment in the form of hotter and drier air blown over the plot-sized wet surface, thus, increasing its evaporation rate. The same effect is negligible on a wet land of regional extent as the originally hot and dry air becomes ever cooler and wetter along its trajectory over the expansive wet surface until it blends completely into the already cool and moist air of the expansive wet land. While the plot-sized wet surface can hardly influence the physical properties of the air blown over it, the regionally expansive wet land can fully influence and transform it, bringing it into equilibrium with its net energy and surface properties. It follows that in the so-called wet environment of the regionally expansive wet land surface the three evaporation rates (potential, E_p, wet-environment, E_w, and actual, E) become equal. It also follows then that the actual land evaporation rate can be derived from differences in the E_p and E_w terms, i.e., it is expected that the larger this difference, the stronger the oasis effect –therefore the more arid the environment– has become which means a proportionally reduced wet environment evaporation rate as actual evaporation. Different authors came up with different, mostly heuristic, answers to how this rate of reduction should be formulated. See Han and Tian (2020) for a brief review on the history of the CR theory.

The heuristic formulation of the CR, however, can be augmented (or completely replaced) by a physically based one, when taking into consideration that the moisture content of the air during wetting and drying cycles of the environment is explicitly related to its temperature under a constant (in a daily or longer averaging sense) wind and energy, Q_n [$= R_n - G$, where R_n (W m^{-2}) is the net surface radiation and G (W m^{-2}) soil heat flux into the ground], available at the surface for latent (i.e., evaporation) and sensible heat (H) fluxes. For possible objections that these two requirements (i.e., temporally constant Q_n and horizontal wind speed) are right away untenable as both wind and surface-available energy are affected by drying/wetting of the environment, it is worth to mention that the only measurements employed in the CR in general come from just one type of actual (typically drying) conditions. No simultaneous –wet *and* drying environment– measurements of any kind are ever employed, so that the wet- or drying-environment data could come from disturbed environmental conditions (meaning wind and Q_n) different from those observed in the actual drying/wet environment, thus not being representative of the actually observed conditions. In other words, the physical reasoning in what follows employs a 'hypothetical' (as long as drying conditions prevail, otherwise the 'hypothetical' becomes what is being measured) wet-environment evaporation term valid strictly under the measured (typically) drying environment Q_n and wind conditions, as base of reference. Therefore, the question whether wetting/drying-cycle constancy of the Q_n and wind terms actually holds true or not in nature is irrelevant.

Below a derivation, giving rise to a physical foundation of the CR, is given. The water-phase diagrams build upon the work of Monteith (1981), Szilagyi and Jozsa (2008), Szilagyi (2014), and Qualls and Crago (2020). Corresponding states (i.e., points given by temperature and vapor-pressure coordinates) along the resulting adiabatic lines (i.e., isenthalps) are related to different evaporation terms. The CR emerges by considerations about the mean speed the corresponding isenthalps are traveled at during a complete dry-out of the environment from a fully wet starting condition. The resulting equation then is written in different forms by employing various wet-surface evaporation rates. Realistic boundary conditions are also introduced to account for possible changes in the mean speed the isenthalps are traveled at during a dry-out. Finally, the different versions of the CR equations are tested with eddy-covariance measurements.

2. Theory: Thermodynamic pathways of an air layer in contact with the evaporating surface

2.1. Derivation of the isenthalps

Let us consider the air layer that extends from the vegetated (i.e., canopy) surface to the height of measurements, z_m, which can be a few meters to possibly up to several tens of meters above the surface. Let the surface receive a temporally constant energy, Q_n (W m^{-2}), available for sensible, H (W m^{-2}), and latent heat, LE (W m^{-2}) fluxes under a steady wind profile. The latent heat flux can be expressed as $LE = L_v \rho_w E$, where L_v (J kg^{-1}) is the latent heat of vaporization, ρ_w (kg m^{-3}) the density of water, and E (m s^{-1}) is the evaporation rate. Let us assume that the latent and sensible heat fluxes stay constant along any vertical (the sum of them equaling the constant Q_n), which approximately holds true in the lowest part of the neutral atmospheric surface layer (Brutsaert, 1982), leading to adiabatic conditions. Then the temporal rate of change (∂_t) in H defined as

$$H = -c_p \rho K(z) \partial_z \theta(t,z) \quad (1)$$

and LE as

$$LE = -L_v \rho K(z) \partial_z q(t,z) \quad (2)$$

is equal but opposite in sign at any level above the vegetated surface, i.e.,

$$\partial_t H + \partial_t LE = 0 \quad (3)$$

Here c_p (J kg^{-1} K^{-1}) is the specific heat of air at constant pressure [p (hPa)], ρ (kg m^{-3}) air density, K (m^2 s^{-1}) the turbulent diffusivity (assumed to be the same for water vapor and heat exchange). ∂_z denotes differentiation with respect to height above the surface, q (-) the specific humidity of the air, approximately equal to 0.622 e / p, where e (hPa) is the vapor pressure. Finally, Θ (K) is the potential temperature, obtainable as $T_a + gz_m / c_p$ (e.g., Stull, 2000) where T_a (K) is the air temperature measured at z_m and g (m s^{-2}) is the gravitational acceleration. Note that q and Θ (also, e and T) are temporal averages of a suitably chosen relatively short time period (e.g., 20 min) and depend on both time (t) and height (z) above the surface, while K is only a function of height. By inserting the flux expressions Eqs. (1) and (2) into Eq. (3), changing the order of differentiations and integrating with respect to elevation one obtains

$$\frac{0.622 \partial_t e_z}{p} + \frac{c_p \partial_t T_z}{L_v} = F(t) \quad (4)$$

which holds true at any height in any time. $F(t)$ is an unknown function (including being a constant) that may depend only on time. For a physically meaningful solution $F(t)$ must be a constant. The constant must be equal to zero then, otherwise the sum of the T and e values at any height would be a linear function of time (and thus boundless) which violates the constant Q_n assumption at the surface, under which the attainable maximum surface temperature is limited. Thus Eq. (4) transforms into

$$de/dT = -\gamma \quad (5)$$

yielding quasi-straight lines (i.e., adiabats which are also called isenthalps under isobaric conditions) of slope -γ (hPa K^{-1}) in the e versus T phase diagram (Fig. 1). Here γ [= $c_p p$ / (0.622L_v)] is the so-called psychrometric constant. Its minor temperature dependence (due to the L_v term) is neglected in this study. Eq. (5) says that changes in vapor pressure (as a result of changing evaporation rates at the land surface) are strictly tied to changes in air temperature under adiabatic and isobaric conditions.

Fig. 1 depicts the two isenthalps in the water phase-diagram, the lower one [from here on referenced as 'air isenthalp' after Qualls and Crago (2020)] at the measurement height, z_m, the other at the surface (upper one). Note that for larger measurement heights all measured temperature values are ought to be converted to potential temperatures and all ensuing calculations performed with those converted values. This way Fig. 1 is strictly valid for measurements at a few meters above the surface.

2.2. Important points of the isenthalps

At the air isenthalp, the minimum temperature achievable by evaporating water into the air is given by the wet-bulb temperature (T_{wb}) obtainable from (Monteith, 1981; Szilagyi, 2014)

$$\frac{e_{wb} - e_a}{T_{wb} - T_a} = -\gamma \quad (6)$$

where e_a and T_a the measured vapor pressure and air temperature while $e_{wb} = e^*(T_{wb})$ the saturation vapor pressure at T_{wb}. Eq. (6) is implicit for T_{wb}, and can be solved by iterations, using, e.g. the Teten's formula for the saturation vapor pressure: $e^*(T) = 6.108\exp[17.27\ T/(237.3 + T)]$ where T is supplied in degree centigrade. Note that $e_a = e^*$ (T_d) where T_d is the dew-point temperature. On the other extreme, the highest temperature (T_a^{dry}) under a constant Q_n is obtained when the air becomes devoid of moisture yielding (Szilagyi et al., 2017; Szilagyi, 2018)

$$T_a^{dry} = T_{wb} + \frac{e_{wb}}{\gamma} = T_a + \frac{e_a}{\gamma} \quad (7)$$

For placement of the surface isenthalp, the wet-surface temperature (T_{ws}) can be used. Szilagyi and Schepers (2014) demonstrated that the wet-surface temperature is independent of the areal extent of the wet surface, thus it can be estimated for a plot-sized wet patch that can only slightly influence the temperature and humidity of the overpassing air. By assuming also that Q_n of the drying land is approximately valid for the wet patch, one can write out the Bowen-ratio, Bo, (=H / LE) as follows (Szilagyi and Jozsa, 2008)

$$\frac{H}{LE} = \frac{Q_n - E_p}{E_p} \approx \gamma \frac{T_{ws} - T_a}{e^*(T_{ws}) - e_a} \quad (8)$$

where Q_n now is expressed in water equivalents of mm d^{-1}, and the above estimate of T_{ws} is denoted by T_{ws}^{SJ} from here on. When T_{ws} is discussed below in general, then the superscript is omitted. Eq. (8) is another implicit equation (for T_{ws}), similar to Eq. (6). The evaporation rate of the wet patch can be obtained by the Penman equation (1948) as

$$E_p = \frac{\Delta Q_n}{\Delta + \gamma} + \frac{\gamma f_u [e^*(T_a) - e_a]}{\Delta + \gamma} \quad (9)$$

where the empirical wind function, f_u (mm d^{-1} hPa^{-1}), is traditionally given by (Brutsaert, 1982) $f_u = 0.26(1 + 0.54u_2)$. Here u_2 (m s^{-1}) is the horizontal wind speed at 2 m. It can be estimated by a power function (Brutsaert, 1982) from measurements (u_h) at h meters above the surface as $u_2 = u_h(2 / h)^{1/7}$. Δ denotes the slope of the saturation vapor pressure curve at the measured temperature T_a. A possible correction to the T_{ws}^{SJ} value, as was recently suggested by Qualls and Crago (2020), is discussed in Appendix I.

The maximum achievable surface temperature (T_s^{dry}) can be obtained from Eq. (7) by replacing T_{wb} with T_{ws}^{SJ}.

In Fig. 1, different evaporation rates can be defined (Qualls and Crago, 2020) if Eq. (2) is divided by $L_v \rho_w$ and finite differences are employed, i.e.,

$$E = -\frac{0.622\rho}{p\rho_w} K(z) \partial_z e \approx -\frac{0.622 K(z_m)}{R_d T \rho_w z_m} (e_a - e_s) \approx f_w (e_s - e_a) \quad (10)$$

where R_d is the gas constant of dry air (287 J kg^{-1} K^{-1}) and f_w (m s^{-1} Pa^{-1}) is a general wind function. When e_s (i.e., the vapor pressure at the surface) is e_{ws} [=$e^*(T_{ws})$], then Eq. (10) yields E_p, and the vertical projection of the corresponding dotted E_p line of Fig. 1 is directly proportional to this value. With the same e_s but e_a is replaced by zero (i.e., dry-environment case), it yields E_p^{dry}. Note that this latter is true as T_{ws} stays constant under a constant Q_n and unchanging wind conditions (Monteith, 1981; Szilagyi, 2014). Note also, that for E_p and E_p^{dry} the corresponding sensible heat fluxes (the horizontal projections of the dotted lines) may become negative, as the air temperature of the drying environment (T_a) can be larger than the surface temperature (T_{ws}) of the plot-sized wet patch, and as a consequence the wet-patch evaporation rates (E_p, E_p^{dry}) may be enhanced by this downward heat transport to exceed the evaporation rate of the wet-environment (i.e., $E_p^{dry} \geq E_p \geq E_w$). An unchanging wet-surface temperature during drying of the environment cannot be assumed for above-ground evaporation pans where the pan is also heated through its side by the sun and the colliding warming air (Szilagyi and Jozsa, 2008) or for bare soil where the sun and warming air heats the dry surface granules of the soil surrounding the wet pores (Aminzadeh et al., 2016).

Qualls and Crago (2020) argue that from the wet endpoint [i.e., from (T_{ws}, e_{ws})] of the surface isenthalp the other wet endpoint (T_{wb}, e_{wb}) of the air isenthalp cannot be reached in a constant flux layer, as the latter requires that the ratio of the two fluxes is constant which takes place

along straight (dotted) lines in the phase diagram of Fig. 1. The lowest such air temperature can be obtained from the intersection of the line tangent to $e^*(T_{ws})$ [with a corresponding slope of $\Delta(T_{ws})$] and the air isenthalp. They also argue that a relatively dry and warm air entraintment at the top of the boundary layer (Lhomme, 1997) with the consequent vertical mixing warms and dries the air above the ground, thus depressing the vapor pressure along the air isenthalp to e_{PT}^{Q} in Fig. 1, with the corresponding elevated air temperature of T_{PT}^{Q}. Here T_{PT} is the wet-environment air temperature while e_{PT} the corresponding vapor pressure, and the superscript 'Q' designates their estimate by Qualls and Crago (2020). Later an alternative estimation of T_{PT} (and e_{PT}) will be introduced.

Qualls and Crago (2020) argue that the effect of air entraintment can be accounted for by multiplying the slope, $\Delta(T_{ws})$, of the line tangent to $e^*(T_{ws})$ with a constant c (>1). The value of c can be obtained by writing Bo as γ / [$c\Delta(T_{ws})$] in the near saturated air layer of a wet environment, rearranging it for E [= Q_n / (1 + Bo)] and equaling it to the wet-environment evaporation rate (Priestley and Taylor, 1972) of

$$E_w = \alpha \frac{\Delta(T_{ws}) Q_n}{\Delta(T_{ws}) + \gamma} \tag{11}$$

where α (>1) is the dimensionless Priestley-Taylor coefficient, also accounting for the boundary-layer air entraintment. The result becomes (Qualls and Crago, 2020)

$$c = \frac{\alpha\gamma}{\Delta(T_{ws})(1-\alpha) + \gamma} \tag{12}$$

The wet-environment evaporation rate of Eq. (11) then can also be expressed by Eq. (10) with the help of e_{ws} and e_{PT}^{Q} (Fig. 1), the latter as the intersection of the air isenthalp with the $c\Delta(T_{ws})$ line (see later).

2.3. Estimation of actual evaporation rates

For the actual evaporation rate, E, the point, (T_s, e_s), on the surface isenthalp that links with (T_a, e_a) on the air isenthalp must be located. This can be achieved from the observation that during a complete drying out of the environment from fully wet conditions, the (T_s, e_s) and the corresponding (T_a, e_a) states/points travel down the whole length of the respective isenthalps, reachable in a constant-flux layer with entraintment, i.e., from (T_{ws}, e_{ws}) down to (T_s^{dry}, 0) on the surface isenthalp, and from (e_{PT}^{Q}, T_{PT}^{Q}) to (T_a^{dry}, 0) on the air isenthalp (Fig. 1). Since later on an alternative definition of T_{PT} and e_{PT} is given, and what follows is equally true for those alternative estimates, reference to the type of T_{PT} and e_{PT} estimate is dropped from here on except when it becomes important which estimate is considered.

As the two isenthalp sections have different lengths, the average speed they are fully travelled down at are different, but their ratio is constant (>1, since the saturation vapor pressure curve is a monotonically increasing function with temperature), and the same constant under unchanging Q_n and wind conditions. By assuming, as a first approximation, that this constant ratio of the average velocities holds true any time during a dry out, then the same applies to the distances travelled. Note, it does not mean that drying out of the environment would happen at a constant speed along the isenthalps, it only means that the distance the phase diagram coordinate point on the surface isenthalp reaches by any time from its wet starting point is larger than the one on the air isenthalp by the same constant percentage. As the slopes of the two isenthalps are identical (forming similar right-angled triangles) the two ratios of e_a / e_{PT} and e_s / e_{ws} must also be equal. Similar expressions can be written for the corresponding temperatures, additionally involving T_a^{dry} and T_s^{dry}.

The

$$\frac{e_a}{e_{PT}} = \frac{e_s}{e_{ws}} \tag{13}$$

relationship, can equally be written as

$$\frac{e_a}{e_{PT}} = \frac{e_{ws} - (e_{ws} - e_a)}{e_{ws} - (e_{ws} - e_{PT})} = \frac{e_s}{e_{ws}} \tag{14}$$

From Eq. (13) the right-hand-side of Eq. (14) can also be written as

$$\frac{e_s}{e_{ws}} = \frac{e_s(1 - \frac{e_a}{e_s})}{e_{ws}(1 - \frac{e_a}{e_s})} = \frac{e_s(1 - \frac{e_{PT}}{e_{ws}})}{e_{ws}(1 - \frac{e_{PT}}{e_{ws}})} = \frac{e_s - \frac{e_s}{e_{ws}} e_{PT}}{e_{ws} - e_{PT}} = \frac{e_s - e_a}{e_{ws} - e_{PT}} \tag{15}$$

By combining Eqs. (14) and (15) one obtains

$$\frac{e_s - e_a}{e_{ws} - e_{PT}} = \frac{e_{ws} - (e_{ws} - e_a)}{e_{ws} - (e_{ws} - e_{PT})} \tag{16}$$

which, with the help of Eq. (10) and Fig. 1, yields a linear non-dimensional equation (Crago and Qualls, 2018)

$$\frac{E}{E_w} = \frac{E_p^{dry} - E_p}{E_p^{dry} - E_w} \tag{17}$$

which upon rearrangement and division by E_p transforms into

$$\frac{E}{E_p} = \frac{E_p^{dry} - E_p}{E_p^{dry} - E_w} \frac{E_w}{E_p} \tag{18}$$

E_p^{dry} can be calculated from Eq. (9) with the $e_a = 0$ and $T_a = T_a^{dry}$ substitutions, plus Δ evaluated at T_a^{dry}. The right-hand-side of Eq. (17) can be considered as an instantaneous wetness index (w) with values between zero (under extremely dry conditions) and unity (in a wet environment).

Eq. (18) can be written in a more succinct, non-dimensional form as

$$y = X \quad \text{with} \quad y = \frac{E}{E_p};\ X = \frac{E_p^{dry} - E_p}{E_p^{dry} - E_w} \frac{E_w}{E_p} \tag{19}$$

From Eq. (16) and Fig. 1 y and X can be equally expressed with only the vapor pressure terms as

$$y = \frac{e_s - e_a}{e_{ws} - e_a} \quad \text{and} \quad X = \frac{e_a}{e_{PT}} \frac{e_{ws} - e_{PT}}{e_{ws} - e_a} \tag{20}$$

Note that $w = e_a$ / e_{PT} now. Actual evaporation rates then can be estimated in several ways.

The first such approach is when one employs only the vapor pressure terms (or equally temperature ones, but this latter approach would also require the T_a^{dry} and T_s^{dry} values) without explicit reliance on Eq. (9) or Eq. (11). From the definition of Bo, one can write $E = Q_n$ / (1 + Bo), i.e.,

$$E = \frac{Q_n}{1 + \gamma \frac{T_s - T_a}{e_s - e_a}} \tag{21}$$

in which e_s from Eq. (13) becomes

$$e_s = e_{ws} \frac{e_a}{e_{PT}} \tag{22}$$

where e_{PT} can be obtained from elementary coordinate geometry of finding the intersection of the air isenthalp [$e = \gamma(T_a - T) + e_a$] and the $c\Delta$ (T_{ws}) tangent line [$e = c\Delta(T_{ws})(T - T_{ws}) + e_{ws}$] yielding

$$T_{PT} = \frac{c\Delta(T_{ws})T_{ws} + \gamma T_a + e_a - e_{ws}}{c\Delta(T_{ws}) + \gamma} \tag{23}$$

and thus

$$e_{PT} = \gamma(T_a - T_{PT}) + e_a \tag{24}$$

The unknown T_s in Eq. (21) drops out from the surface isenthalp equation as

$$T_s = T_{ws} + \frac{e_{ws} - e_s}{\gamma} \tag{25}$$

Note that Eq. (21) does not contain any explicit wind reference, but implicitly it is present in the estimation of T_{ws} via Eqs. (8) and (9). Crago and Qualls (2018) found that Eq. (19) worked well for diverse (grass, wetland, bush, savanna, forest) eddy-covariance measurement locations

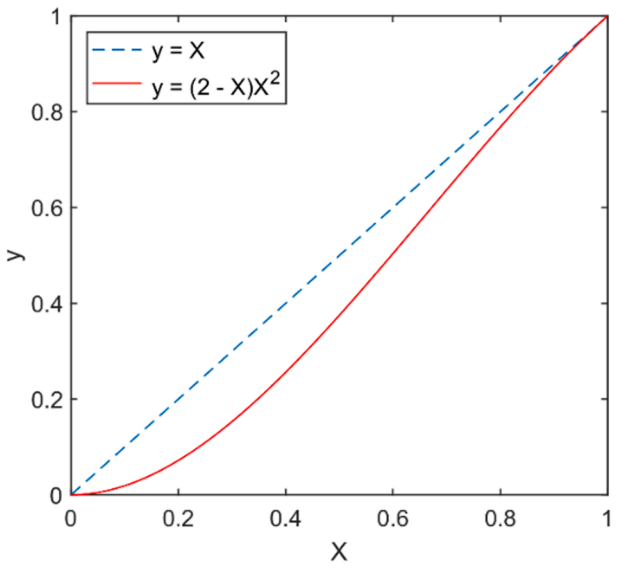

Fig. 2. The linear and nonlinear CR relationships between $y = E / E_p$ and $X = w$ E_w / E_p. The nonlinear approach builds upon the work of Brutsaert (2015) with improvements in the scaled variables by Szilagyi et al. (2017).

in Australia. The present vapor-pressure-based approach of Eq. (21) eliminates any potential uncertainties associated with the estimation of E_p^{dry}.

Szilagyi et al. (2017), Szilagyi (2018), Ma and Szilagyi (2019), and Ma et al. (2019, 2020) found a nonlinear formulation of Eq. (19) very effective with continental-scale gridded input data of monthly T_a, T_d, Q_n, and u_{10} values. The nonlinear version follows from considerations about the relative changes (dy and dX) in y and X of Eqs. (19) and (20) at $w = 0$. Writing $dy = dE/dE_p = (de_s - de_a)/dE_p$ and $dX = (de_a/e_{PT})E_w/dE_p$, one obtains $dy/dX = [(de_s - de_a)/de_a]e_{PT}/E_w$ where e_{PT} and E_w are constant during isenthalpic processes. Thus, dy/dX vanishes provided the terms in the bracket do the same, requiring $de_s/de_a \approx (e_s|_{w>0} - e_s|_{w=0})/(e_a|_{w>0} - e_a|_{w=0}) = 1$. Considering that at $w = 0$ both e_s and e_a are zero theoretically, this is equivalent to the condition of $e_s \approx e_a$ following wetting the dry surface for an infinitesimally short period of time. But this can exactly be expected as a small quantity of moisture introduced onto the dry surface will require only a negligible vertical gradient in atmospheric humidity to diffuse practically evenly within the turbulent boundary layer resulting in a quasi-constant vertical humidity profile. For a practical illustration of this taking place, see the average vertical profile of the specific humidity in Fig. 5a in Mamtimin et al. (2020) obtained at 4 p.m. each day in the winter of 2017 over a desert area in China. In the winter the desert is covered in a thin layer of snow (partly the result of dry deposition during the extreme cold winter nights) but a small quantity of meltwater may occur for a short period of time even in subzero temperatures due to strong daytime irradiation, creating brief wet pulses in the afternoons of sunny days, mimicking the wetting requirement described above (with the obvious difference that evaporation is limited not by the lack of moisture at the surface but instead by subzero temperatures during most of the day) and resulting in a practically constant afternoon vertical moisture profile.

The ensuing nonlinear form of Eq. (19) can thus be written as

$$y = (2 - X)X^2 \tag{26}$$

See Ma and Szilagyi (2019) for more details about the nonlinear approach. This nonlinear approach of Eq. (26) can now be applied where X and y are defined by Eq. (20) and the resulting e_s inserted into Eq. (21).

The Bowen-ratio term of Eq. (21) may cause problems with inaccurate measurements, especially when e_s is close to e_a. Therefore, for practical applications it may be better to employ a hybrid approach that would contain both, flux and vapor pressure, terms. By keeping the vapor pressure formulation of the wetness index, $w = e_a / e_{PT}$, in Eq. (20), and inserting it into X of Eq. (19) or Eq. (26) with $y = E / E_p$, a linear

$$\frac{E}{E_p} = \frac{e_a}{e_{PT}} \frac{E_w}{E_p} \tag{27}$$

or nonlinear

$$\frac{E}{E_p} = \left(2 - \frac{e_a}{e_{PT}} \frac{E_w}{E_p}\right)\left(\frac{e_a}{e_{PT}} \frac{E_w}{E_p}\right)^2 \tag{28}$$

hybrid approach is defined where Eq. (21) is no longer needed.

The nonlinear approach relaxes the constant relative mean speed assumption of Eq. (13) and lets the (T_s, e_s) state-point of the surface isenthalp run progressively ahead of the corresponding (T_a, e_a) state on the air isenthalp so that the ratio of distances travelled changes in time. As a consequence, the nonlinear approach always yields smaller

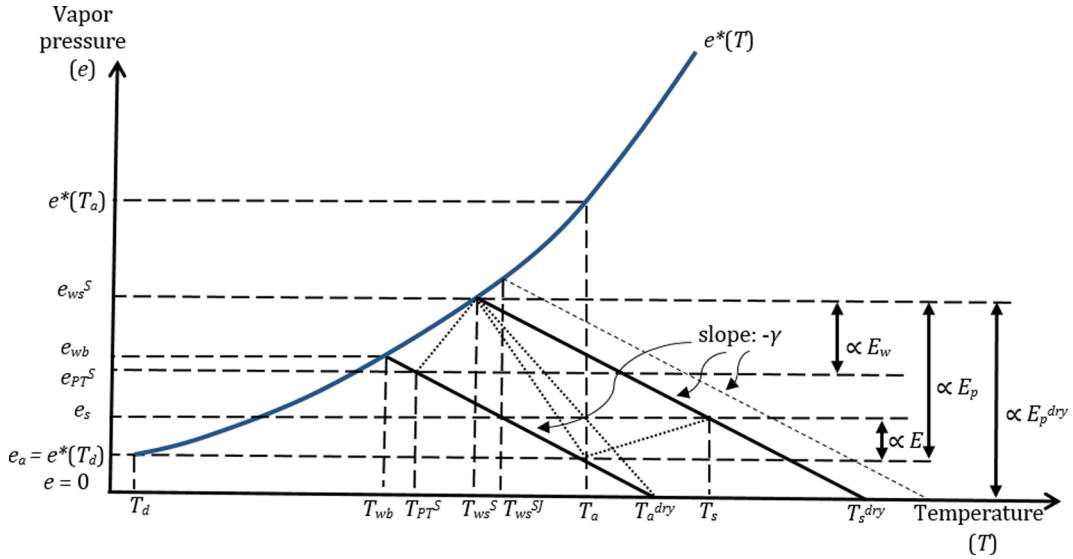

Fig. 3. Schematics of the saturation vapor pressure (e^*) curve, the air (bottom) and vegetated land surface (top) isenthalps of slope $-\gamma$ in a surface layer affected by air entraintment at the top of the boundary layer. The vertical (and horizontal) projections of the four dotted lines are proportional ($\propto$) to the different evaporation (and sensible heat, negative with E_p and E_p^{dry}) rates specified. See Table 1 for the definition of evaporation rates and the relevant temperatures.

evaporation rates than the linear one with the same α value (Fig. 2). The reason of accounting for possible changes in the relative mean speed of the isenthalp coordinates by Eq. (26) rather than taking a nonlinear function of w itself in Eq. (17) is that Eq. (26) does not introduce any additional parameter to calibrate, while taking any nonlinear function of w in Eq. (17) would, as the relative changes of E / E_w and w at the wet and dry end-points of the isenthalps are unknown yet, contrary to the better researched case of y and X in Eq. (26).

Note that the hybrid approaches– Eqs. (27) and (28)– still contain only one parameter to calibrate, the Priestley-Taylor coefficient, α.

Finally, it is also worthwhile to test the CR in a full flux mode [Eqs. (19) and (26)] where all evaporation terms are explicitly given: E_p by Eq. (9), E_w by Eq. (11), E_p^{dry} by Eq. (9) again with $e_a^{dry} = 0$ and T_a^{dry} estimated with the help of Eq. (7) (Szilagyi et al., 2017; Szilagyi, 2018).

2.4. An alternative derivation of the wet-environment air and surface temperature

The wet environment air temperature, T_{PT}, can be obtained by equating the evaporation rate of the Penman equation (Eq. (9)) with that of the Priestley-Taylor equation (Eq. (11)) if in either equation the yet unknown T_{PT} is employed which thus yields an implicit equation for T_{PT}, provided a value for α is set, i.e.,

$$\alpha \frac{\Delta(T_{PT})}{\Delta(T_{PT})+\gamma} Q_n = \frac{\Delta(T_{PT})}{\Delta(T_{PT})+\gamma} Q_n + \frac{\gamma}{\Delta(T_{PT})+\gamma} f_u [e^*(T_{PT}) - e_{PT}] \quad (29)$$

where the estimate of e_{PT} [i.e., e_{PT}^S to differentiate it from a similar estimate of Qualls and Crago (2020)] comes from Eq. (24) with the T_{PT} solution of Eq. (29). Note that the estimate of T_{PT} (i.e., T_{PT}^S) in Eq. (29) is strictly tied to the value of the typically unknown Priestley-Taylor α. The also unknown vapor pressure value at the surface, e_{ws} [as an alternative to $e^*(T_{ws}^{SJ})$ of Eq. (8)], then can be obtained by equating the Priestley-Taylor equation with Eq. (21), both employing T_{PT}^S, such as

$$\alpha \frac{\Delta(T_{PT}^S)}{\Delta(T_{PT}^S)+\gamma} Q_n = \frac{Q_n}{1+\gamma \frac{T_{ws}-T_{PT}^S}{e_{ws}-e_{PT}^S}} \quad (30)$$

which is again implicit for $e_{ws} = e^*(T_{ws})$ and can be solved by iterations.

The resulting estimates of T_{ws} and e_{ws}, i.e., T_{ws}^S, e_{ws}^S, define the surface isenthalp (Fig. 3), which is to the left of the original isenthalp going through $[T_{ws}^{SJ}, e^*(T_{ws}^{SJ})]$.

For the CR theory demonstration below, both wet-environment air temperature (T_{PT}^Q and T_{PT}^S) and wet-surface temperature estimates (T_{ws}^{SJ}, T_{ws}^S) are applied.

3. Results: Demonstration of the CR theory with eddy-covariance measurements

The three versions (Bowen-ratio, hybrid, and full flux) of the CR were tested with eddy-covariance data of seven Australian FLUXNET sites (http://fluxnet.fluxdata.org/sites/site-list-and-pages/). These sites include land covers of grass, permanent wetland, open shrubland, woody savanna, and evergreen broadleaf forests. For more information on the data, stations and their locations, see Crago and Qualls (2018). Measurement heights (for u_2 and Θ) were reduced by the average height of the vegetation. All three CR versions were tested by the wet-environment air temperature, T_{PT}^Q, of Qualls and Crago (2020), and also by T_{PT}^S. Similarly, the two wet surface estimates (T_{ws}^{SJ} and T_{ws}^S) were also tested. Through systematic trial-and-error optimization a PT α value was calibrated by minimizing the root-mean-squares error (RMSE) between model estimates and EC measurements. No correction of any sort was applied for the EC values. Model performance was gauged by simultaneous assessment of the (i) RMSE value; (ii) place the calibrated PT α value occupies within the widely accepted range of (1–1.32); (iii) slope of the sum-of-squares fitted line, and; (iv) shape of the data cloud around the best-fit line. The linear correlation coefficient value (R) was found a weak indicator for additional model performance assessment because it varies little between the model versions. Table 2 summarizes model performances.

As seen in Table 2, the RMSE value improves (from 20.17 to 19.18 mm mo^{-1}) in the linear CR version by a switch from T_{PT}^Q to T_{PT}^S values. The improvement is not sensitive to whether the original e_{ws}^{SJ} or the newly derived e_{ws}^S estimates (Fig. 4) are employed, as model performance practically stays the same with the T_{PT}^S values. The optimized value of α increases from its physically meaningful lower boundary of unity to 1.06 with the T_{PT}^Q to T_{PT}^S switch because the latter values are generally closer to T_{wb}. The unity PT α value in the first case suggests that the linear CR overestimates the evaporation rates by overestimating e_s. This is possible only if the surface isenthalp point cannot satisfactorily run ahead of the air isenthalp point due to the employed constant relative speed assumption. Therefore, calibration will lower the value of α in Eq. (12), thus, pushing the $c\Delta(T_{ws})$ line to the left in Fig. 1, and as a

Table 1
List of the different sensible heat (H) and evaporation (E) rates employed in the study together with the relevant temperatures (T) defined.

E (H)	Actual evaporation [latent heat (LE)] and sensible-heat rate
E_p (H_p)	Potential (Penman) evaporation/sensible-heat rate
E_p^{dry} (H_p^{dry})	Dry-environment potential evaporation/sensible-heat rate
E_w (H_w)	Wet-environment evaporation/sensible-heat rate
T_a	Actual air temperature
T_a^{dry}	Dry-environment air temperature
T_d	Dew-point temperature
T_{PT}	Wet-environment air temperature
T_{PT}^Q	Wet-environment air temperature estimate by Qualls and Crago (2020)
T_{PT}^S	Wet-environment air temperature estimate from Eq. (29)
T_{wb}	Wet-bulb temperature
T_s	Land-surface temperature
T_s^{dry}	Dry-environment land surface temperature
T_{ws}^S	Wet surface temperature estimate from Eq. (30)
T_{ws}^{SJ}	Wet surface temperature estimate by Szilagyi and Jozsa (2008)
T_{ws}^Q	Wet surface temperature estimate by Qualls and Crago (2020)

Table 2
Summary of the CR model performance when the average height of the vegetation is subtracted from the measurement height. See Table 1 for the different evaporation and temperature definitions. RMSE is the root-mean-square-error, α the sum-of-squares calibrated value of the Priestley-Taylor α in Eq. (11). The best performing (either in RMSE and/or the best-fit slope value) model versions' performance metrics are emphasized.

	Eq. (21) with	Linear CR ($y = X$ with Eq. (20))			Nonlinear CR ($y = 2X^2$-X^3 with Eq. (20))		
		RMSE (mm mo^{-1})	Best-fit slope (-)	α (-)	RMSE (mm mo^{-1})	Best-fit slope (-)	α (-)
(a)	e_{ws}^{SJ} & T_{PT}^Q	20.17	0.79	1	20.93	0.97	1.07
(b)	e_{ws}^S & T_{PT}^S	19.09	0.78	1.06	17.78	0.93	1.12
(c)	e_{ws}^{SJ} & T_{PT}^S	19.18	0.79	1.06	18.67	0.96	1.13
	Hybrid, with	Linear CR (Eq. (27))			Nonlinear CR (Eq. (28))		
(d)	T_{PT}^Q & $E_w(T_{ws}^{SJ})$	19.34	0.77	1.01	18.74	0.96	1.09
(e)	T_{PT}^S & $E_w(T_{ws}^S)$	19.3	0.77	1.04	**17.54**	**0.96**	**1.12**
(f)	T_{PT}^S & $E_w(T_{ws}^{SJ})$	19.12	0.77	1.04	17.65	0.96	1.12
(g)	T_{PT}^Q & $E_w(T_{PT}^Q)$	20.05	0.79	1.09	21.62	0.95	1.15
(h)	T_{PT}^S & $E_w(T_{PT}^S)$	19.28	0.79	1.08	18.87	0.98	1.15
(i)	$E_w(T_{ws}^S)$ & T_{PT} to T_{wb} in w	19.45	0.76	1.04	**17.48**	**0.94**	**1.18**
(j)	$E_w(T_{ws}^{SJ})$ & T_{PT} to T_{wb} in w	19.22	0.77	1.06	17.61	0.95	1.19
	Full flux, with	Linear CR (Eq. (19))			Nonlinear CR (Eqs. (26) and (19))		
(k)	$E_w(T_{ws}^S)$	17.59	0.81	1.07	**18.17**	**1.01**	**1.14**
(l)	$E_w(T_{ws}^{SJ})$	**17.18**	**0.83**	**1.08**	18.54	1.01	1.14
(m)	$E_w(T_{PT}^Q)$	21.45	0.82	1.16	28.94	0.92	1.19
(n)	$E_w(T_{PT}^S)$	17.78	0.85	1.13	20.72	1.02	1.18

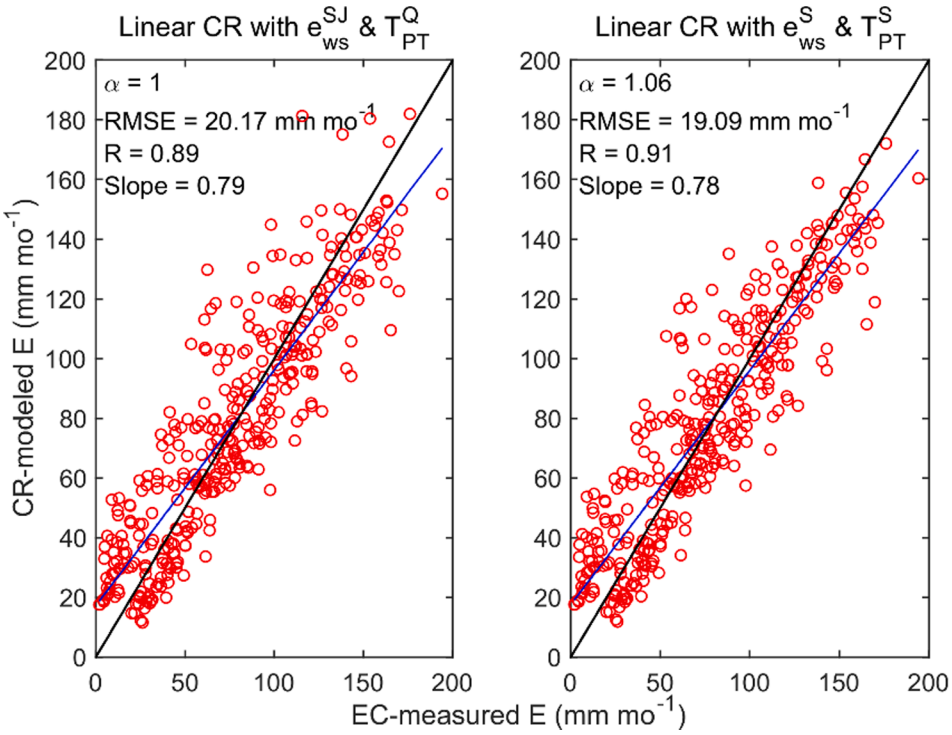

Fig. 4. CR-estimated monthly evaporation rates plotted against eddy-covariance measurements of seven Australian FLUXNET sites. The CR employs either the currently derived wet-environment air temperature (T_{PT}^{S}) together with e_{ws}^{S}, or the one (T_{PT}^{Q}) by Qualls and Crago (2020) with the original e_{ws}^{SJ}. The evaporation estimates come from Eqs. (20) and (21).

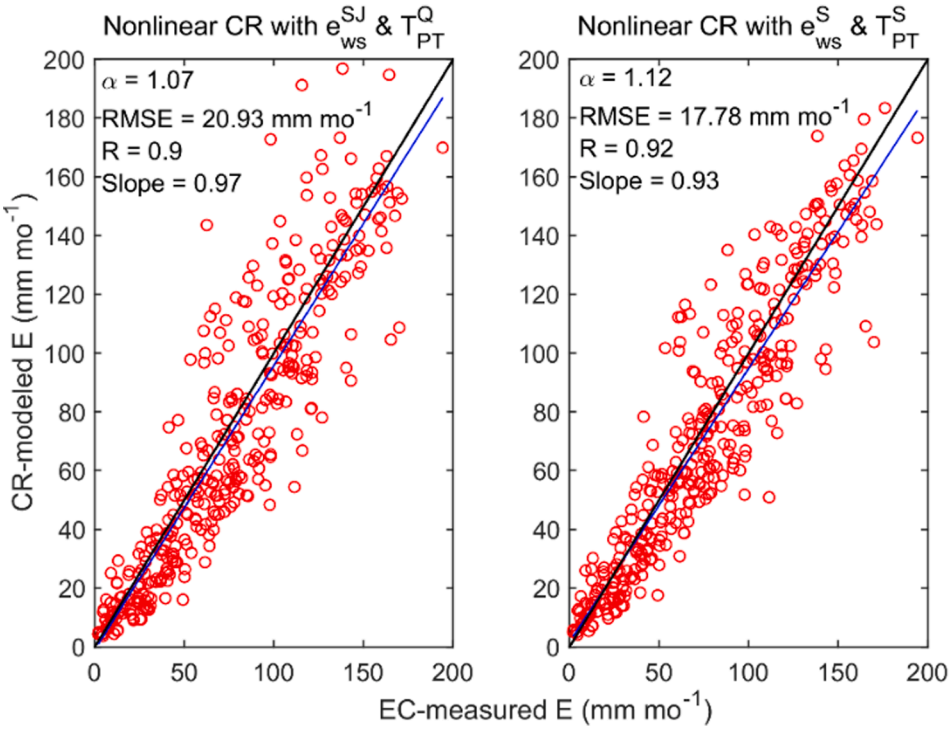

Fig. 5. CR-estimated monthly evaporation rates plotted against eddy-covariance measurements of seven Australian FLUXNET sites. The CR employs either the currently derived wet-environment air temperature (T_{PT}^{S}) together with e_{ws}^{S}, or the one (T_{PT}^{Q}) by Qualls and Crago (2020) with the original e_{ws}^{SJ}. The evaporation estimates come from Eqs. (20), (21) and (26).

consequence, raising the value of e_{PT}^{Q}, which in turn lowers the value of e_s in Eq. (22) which physically means the (e_s, T_s) point is pushed further down the surface isenthalp. The lowered α (=1) value will result in a relatively good performance of the linear CR model, the nonlinear model version employing T_{PT}^{Q} can improve upon only in the slope (0.97 vs 0.79) of the best-fit line (Fig. 5) and in better predicting low values.

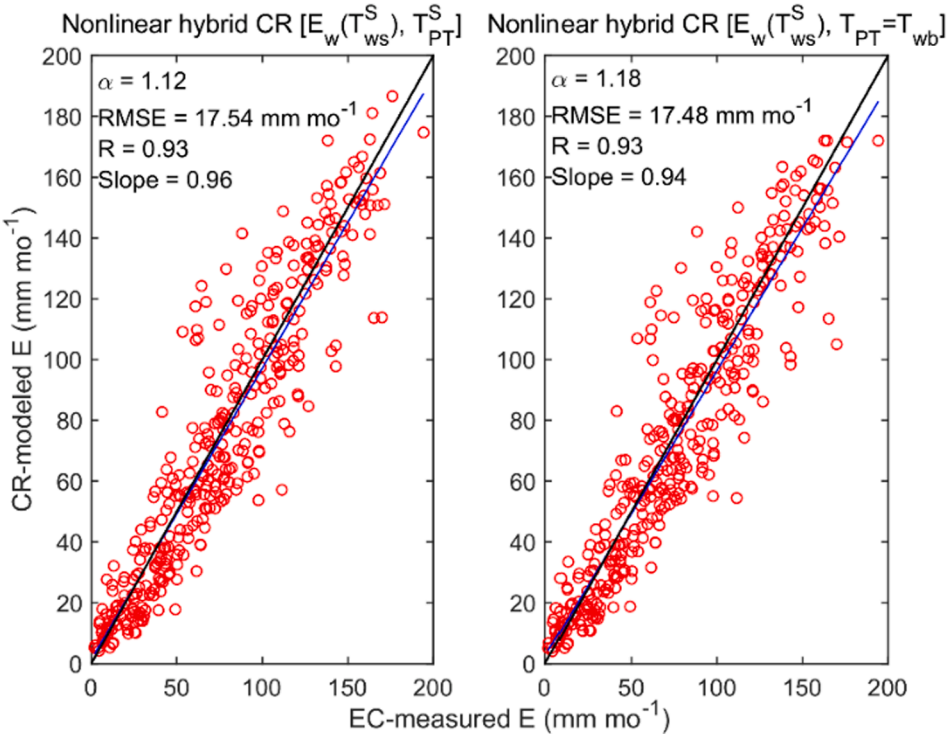

Fig. 6. Monthly evaporation rates by the best (original or hybrid) CR versions plotted against eddy-covariance measurements of seven Australian FLUXNET sites. The CR employs either the currently derived wet-environment air temperature (T^S_{PT}) in the wetness index (w) or its replacement by T_{wb}. The evaporation estimates come from Eq. (28) (nonlinear hybrid).

The T^Q_{PT} to T^S_{PT} switch also improves the estimation in the nonlinear model, evidenced in Table 2 and Fig. 5. Note that the nonlinear model does not need such low α values as the corresponding linear one since it is able to let the surface isenthalp point run ahead more freely, demonstrated by the lower curve (and thus reduced evaporation rate as a result of a more advanced e_s value down the surface isenthalp) in Fig. 2.

With the nonlinear CR version, employing e^S_{ws} and T^S_{PT}, the RMSE

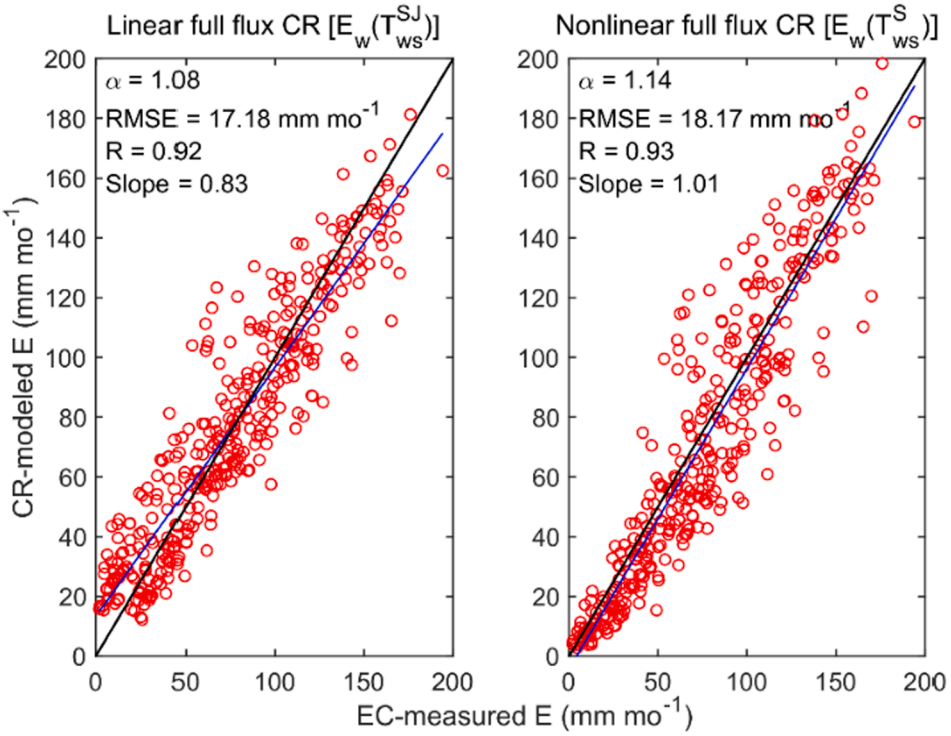

Fig. 7. Monthly evaporation rates by the full flux versions of the CR [Eq. (19) and Eq. (26)] plotted against eddy-covariance measurements of seven Australian FLUXNET sites. E_w is evaluated either at T^{SJ}_{ws} or T^S_{ws}.

Table 3
Summary of the CR model performance employing the original measurement height values with no adjustment for canopy height. See Table 1 for the different evaporation and temperature definitions. RMSE is the root-mean-square-error, α the sum-of-squares calibrated value of the Priestley-Taylor α in Eq. (11). The best performing (either in RMSE and/or the best-fit slope value) model versions' performance metrics are emphasized.

	Eq. (21) with	Linear CR ($y = X$ with Eq. (20))			Nonlinear CR ($y = 2X^2$-X^3 with Eq. (20))		
		RMSE (mm mo^{-1})	Best-fit slope (-)	α (-)	RMSE (mm mo^{-1})	Best-fit slope (-)	α (-)
(a)	e_{ws}^{SJ} & T_{PT}^{Q}	20.41	0.81	1	21.32	0.97	1.06
(b)	e_{ws}^{S} & T_{PT}^{S}	18.97	0.78	1.05	17.65	0.93	1.11
(c)	e_{ws}^{SJ} & T_{PT}^{S}	19.08	0.79	1.05	18.53	0.96	1.12
	Hybrid, with	Linear CR (Eq. (27))			Nonlinear CR (Eq. (28))		
(d)	T_{PT}^{Q} & $E_w(T_{ws}^{SJ})$	19.29	0.77	1	18.84	0.96	1.08
(e)	T_{PT}^{S} & $E_w(T_{ws}^{S})$	19.13	0.77	1.03	**17.4**	**0.96**	**1.1**
(f)	T_{PT}^{S} & $E_w(T_{ws}^{SJ})$	19.01	0.77	1.03	17.48	0.96	1.11
(g)	T_{PT}^{Q} & $E_w(T_{PT}^{Q})$	19.91	0.76	1.05	21.54	0.93	1.13
(h)	T_{PT}^{S} & $E_w(T_{PT}^{S})$	19.1	0.78	1.07	18.65	0.96	1.13
(i)	$E_w(T_{ws}^{S})$ & T_{PT} to T_{wb} in w	19.24	0.76	1.04	**17.2**	**0.94**	**1.17**
(j)	$E_w(T_{ws}^{SJ})$ & T_{PT} to T_{wb} in w	19.07	0.77	1.05	17.28	0.94	1.17
	Full flux, with	Linear CR (Eq. (19))			Nonlinear CR (Eqs. (26) and (19))		
(k)	$E_w(T_{ws}^{S})$	17.52	0.81	1.06	**18.14**	**0.98**	**1.12**
(l)	$E_w(T_{ws}^{SJ})$	**17.19**	**0.83**	**1.07**	**18.5**	**1**	**1.13**
(m)	$E_w(T_{PT}^{Q})$	21.31	0.8	1.14	28.61	1.03	1.22
(n)	$E_w(T_{PT}^{S})$	17.67	0.84	1.12	20.61	1	1.16

value becomes the smallest so far. The small measured EC values at the bottom of the data cloud in Fig. 5 are also captured much better with either T_{PT} value than in the linear model.

When switching to the hybrid model formulation of Eqs. (27) and (28), the slope of the saturation vapor pressure curve, Δ, in E_w of Eq. (11), may be evaluated at different temperatures. Eq. (11) defines the slope at the wet-surface temperature, T_{ws}, but originally, it was defined at the wet-environment air temperature (T_{PT}) by Priestley and Taylor (1972) due to the typical availability of T_{PT} when the measurements are actually carried out under fully wet environmental conditions. Since both, the wet surface and the wet-environment air, temperature (T_{PT}) estimates are available now, it is worth evaluating Eq. (11) at either, wet surface and wet-environment air, temperature.

Model performance was found to improve when the T_{ws} values E_w is evaluated at are capped by the actual dry-environment air temperature (T_a). Normally the wet-surface temperature is below the drying environment air temperature, except when the environment is close to its fully wet state. To be consistent with the Penman equation, Eq. (11) must also be evaluated at the (wet environment) air (as was done by Priestley and Taylor, 1972) and not the surface temperature. The wet surface temperature serves only as a proxy of the typically unknown (i.e., when measurements are coming from a drying environment) wet-environment air temperature, and since this latter is always smaller than the drying environment air temperature due to the energy requirement of evaporation, the T_{ws} values must be capped by T_a. Note that the T_{PT} values are tied to the PT α values [via Eqs. (12) and (23) for T_{PT}^{Q} and via Eq. (29) for T_{PT}^{S}], therefore the latter cannot be calibrated independent of T_{PT} as it can be done when Eq. (11) is evaluated at T_{ws} instead of T_{PT}.

As seen in Table 2, the linear hybrid model generally performs the same way as before, with typically low calibrated α values. A real improvement takes place (RMSE = 17.54 mm mo^{-1}, best-fit slope of 0.96) in the nonlinear model (Fig. 6), when Eq. (11) is evaluated at the wet surface temperature (T_{ws}^{S}) and the wetness index, w (=e_a / e_{PT}), is expressed with T_{PT}^{S}. A similar performance is seen (RMSE = 17.48 mm mo^{-1}, best-fit slope of 0.94) when the wet-environment air temperature, T_{PT}, is replaced by the wet-bulb temperature in the wetness index, i.e., $w = e_a / e_{wb}$. This again indicates that the T_{PT}^{S} values are generally closer to the wet-bulb temperatures than the T_{PT}^{Q} estimates. Note that in all cases so far [cases (a) vs (c), (d) vs (f), (g) vs (h), (m) vs (n) in Table 2], the T_{PT}^{S} estimates produced better performance than the T_{PT}^{Q} ones.

When the CR is applied in its full flux mode, the best model performance (RMSE = 17.18 mm mo^{-1}) is provided by the linear model version (Table 2 and Fig. 7), however the best-fit line's slope still remains relatively low (0.83) and the smallest values are greatly overestimated.

The best nonlinear full flux CR model versions (RMSE = 18.17 mm mo^{-1} and RMSE = 18.54 mm mo^{-1}) improve model sensitivity (Fig. 7), yielding an almost perfect best-fit line slope of unity with E_w evaluated at T_{ws}^{S} or at T_{ws}^{SJ}, respectively (Table 2). On average T_{ws}^{S} is smaller than T_{ws}^{SJ}, but the difference is only 0.1 °C. The calibrated PT α (=1.14) value in either model versions is almost identical to what was reported ($\alpha = 1.15$) by Szilagyi et al. (2017) using the same monthly full flux model with gridded data over the coterminous United States. Model estimates are about 4 mm mo^{-1} (i.e., 5%) below the EC measurements on average by these best performing nonlinear full flux model versions.

The results considered so far employed a measurement height that was reduced by the average height of the vegetation, something that is not routinely known for natural land covers. To see how the lack of this information affects modeling results, all calculations were repeated using the original measurement height values. Table 3 lists the so-derived performance statistics. The differences are generally small because for forests where the measurement height differences are the largest the empirical wind function in the Penman equation is only mildly sensitive to wind speed differences as wind-speed itself changes little vertically at those heights. In other sites, where the vertical wind profile closer to the surface changes more rapidly, the vegetation height itself is small.

As seen, all of the general conclusions drawn thus far still remain valid as the numerical values change only slightly with a few exceptions only. This is in support of a routine application of the CR with gridded basic meteorological data where typically land cover information is missing.

4. Summary

With the help of the water phase-diagram under isenthalpic (i.e., isobaric and adiabatic) drying/wetting cycles of the environment, and also assuming unchanging wind conditions, states [i.e., successive (e, T) points] along the surface isenthalp were linked to similar states along the air isenthalp, the latter representing the measurement height. The linkage was based on the constant relative speed assumption which surmises that the states evolve along the respective isenthalps during drying/wetting cycles so that the scaled distances (i.e., distance travelled from an endpoint of the isenthalp divided by the total length of the isenthalp) are equal between the isenthalps. The isenthalps were represented by straight lines of slope -γ on the phase-diagram, which is an acceptable approximation under naturally occurring environmental conditions. The linked vapor pressure terms, thus, define different evaporation rates up to a near-constant multiplier of a general wind function (Eq. (10)), the latter incorporating the turbulent diffusivity and the measurement height. The placing (i.e., horizontal or vertical distance) of the two isenthalps depends only on the (i) available energy at the surface; (ii) wind function, and; (iii) measurement height; and it can be located with the help of the Priestley-Taylor and Penman equations as was demonstrated above.

Actual evaporation rates were first estimated by only the measured air temperature and vapor pressure, together with the estimated surface temperature and vapor pressure values via Eq. (21). The latter requires the maximum value the vapor pressure may assume (e_{PT}) at the measurement height and it was estimated by Eqs. (23) and (24), recommended by Qualls and Crago (2020), and by a different approach described above, i.e., with the help of Eqs. (29) and (24).

By assigning evaporation rates (E, E_p, E_p^{dry}, E_w) to the different air and surface vapor-pressure combinations, an existing linear CR model [i.e., that of Crago and Qualls (2018)] emerges naturally from the constant relative speed assumption.

The constant relative speed assumption then was relaxed with the help of a nonlinear relationship (Szilagyi et al., 2017) among two scaled (nondimensional) evaporation terms, $y = E / E_p$, and $X = w\ E_w / Ep$, where w is a wetness index, to yield a nonlinear CR.

Both the linear (i.e., $y = X$) and nonlinear [i.e., $y = (2 - X)X^2$] CR models (first containing only vapor pressure and temperature terms) were tested by monthly aggregated EC measurements of seven Australian FLUXNET sites. The nonlinear model gave better evaporation estimates in terms of the RMSE value and model sensitivity (expressed in best-fit line slopes close to unity) (Table 2) in comparison with the linear model, the latter ending up overestimating the small values and underestimating the large ones (Fig. 4). The wet environment air temperature estimation of Eq. (29) (T_{PT}^S) helped with improving the RMSE value and model sensitivity (Table 2).

Next, in the hybrid approach, E_p and E_w were expressed by the corresponding flux equations [Eqs. (9) and (11)], while the wetness-index was kept in its vapor pressure formulation of $w = e_a / e_{PT}$. E_w then was evaluated with two alternative wet-surface (capped by T_a) and also with two wet-environment air temperature estimates. The linear model gave similar evaporation estimates with typical low model sensitivity (expressed in low values of the best-fit line). The nonlinear model improved model performance (except with T_{PT}^Q in E_w) leading to significantly better overall sensitivity (reaching a best-fit slope of 0.96).

In the next step, the wet-surface temperatures were kept for evaluating E_w, and it was tested if replacing T_{PT} by the wet-bulb temperature (T_{wb}) in the wetness index –as the lowest achievable air temperature by evaporating water into the air, typically provided by psychrometers or estimated by Eq. (6)–, would result in better predictions. Neither the linear nor the nonlinear model responded much, which suggests that the hybrid model is more sensitive to whether the model is linear or not than to which T_{PT} estimate the wetness index contains once E_w is evaluated at T_{ws}.

In the final step of CR theory demonstration, the wetness index was also expressed by explicit flux terms, leading to the best overall RMSE value of 17.2 mm mo^{-1} in the linear model but still accompanied by low model sensitivity. Note that the T_{PT} values now are present only optionally (in place of T_{ws}) in the E_w term. The full flux model formulation lead to a somewhat larger RMSE value in the nonlinear approach but yielded practically perfect best-fit line slope of unity with E_w evaluated at the alternative wet-surface temperatures. The full flux model only slightly worsened when T_{ws} was replaced by T_{PT}^S for the E_w evaluation but deteriorated significantly (especially in the nonlinear case) with T_{PT}^Q, reinforcing that the T_{PT}^S estimates are physically more realistic than the T_{PT} estimates of Qualls and Crago (2020).

The flux formulation of the wetness index seems to be more sensitive to changes in environmental aridity than the vapor pressure one. This may be the reason for an improved CR model response in the RMSE and best-fit slope values for the linear version and in the latter only for the nonlinear one. This improved sensitivity may occur because the Penman equation contains the vapor pressure deficit, which is highly responsive to changes in air temperature (as a response to surface wetness) due to the steep slope of the saturation vapor pressure curve, especially at higher temperatures. Even though the RMSE indicator did not improve for the nonlinear model, the best-fit slope did so, yielding an almost perfect value of unity. Similar observations about the two versions of the wetness index (vapor pressure or flux) have already been made by Szilagyi et al. (2017) with continental-scale gridded data.

As seen, the CR model is not sensitive to the location of the surface isenthalp (compare Table 2 and 3), therefore canopy height of the vegetation is not required to be known which is a great advantage in large scale model applications employing gridded data. Neither is the CR model sensitive to the type of wet-surface temperature estimate (T_{ws}^{SJ} vs T_{ws}^S) which is again advantageous as this way the Priestley-Taylor α can be estimated calibration-free and separately of the CR application, as was demonstrated by Szilagyi et al. (2017) and Szilagyi (2018) for the conterminous United States, and by Ma et al. (2019) for China. Also, the demonstrated best sensitivity of the full flux model further justifies its previous very effective continental-scale applications (most recently by Szilagyi et al., 2020) in cases where aridity is changing on a wide scale.

5. Conclusions

All in all, this study revealed a physical foundation for the complementary relationship of evaporation with the help of defining the thermodynamic pathways the air at the vegetated surface and at the measurement height may follow under simplified atmospheric (isobaric and adiabatic) conditions. Certainly, such conditions may be violated in the real atmosphere, but typically not to such a degree that would invalidate the CR theory as a whole, as it is proven by its practical success, outperforming or matching existing, often complex, and data intensive, large-scale evaporation estimation methods (Szilagyi, 2018; Ma and Szilagyi, 2019; Ma et al., 2019, 2020). As about the linearity vs nonlinearity dilemma of the CR, the present study confirmed earlier findings by Han et al. (2012) and Szilagyi (2018) that a nonlinear formulation can be expected to result in more realistic evaporation estimates, expressed in best-fit line slope values close to unity.

Hopefully the detailed physical approach on the foundation of the CR discussed in this study will lead to wider application of the method for estimating land evaporation rates on a weekly, monthly, annual bases. This is expected to happen as the method can be made calibration-free (i.e., full flux version with E_w evaluated at T_{ws}^{SJ}) at large spatial scales where the value of its sole (temporarily and spatially constant) parameter, the Priestley-Taylor α, can be set by the method of Szilagyi et al. (2017) requiring no ground-truth measurements of evaporation or application of water balances. Due to its minimal data requirement (air temperature and humidity, horizontal wind speed, and net surface radiation, an estimate for the latter also obtainable from sunshine duration data) it can provide land evaporation estimates over longer historical periods than probably any other existing physically-based method. Notice that it requires no precipitation information at all.

The CR is not recommended to be routinely applied at a daily scale and near sudden jumps of wetness conditions (e.g., near sea-shores) where the moisture of the air may not be representative of the underlying land surface either temporarily due to a passing weather front or permanently due to existing diurnal land-sea breezes.

Declaration of Competing Interest

The authors declare that they have no known competing financial interests or personal relationships that could have appeared to influence the work reported in this paper.

Acknowledgements

I would like to thank R. Crago for providing the Australian FLUXNET data in an Excel-organized format. This research was supported by the BME Water Sciences & Disaster Prevention TKP2020 IE grant of NKFIH Hungary (BME IE-VIZ TKP2020).

Appendix I

Qualls and Crago (2020) argue that the T_{ws} value obtainable from Eq. (8) is incorrect as the Δ term in Eq. (9) is evaluated at (the known) T_a and not at (the typically unknown) T_s, as it ought to be. They overlook the possibility that the T_s to T_a switch could be corrected, at least to some degree, by a properly chosen wind function in Eq. (9). They argue that the "correct" surface isenthalp must go through the intersection of the E_p line [i.e., the solid line between (T_a, e_a) and (T_{ws}^{SJ}, e_{ws}^{SJ}) in Fig. A1] and the line tangent $\Delta(T_a)$, resulting in the sample (T_s^{Δ}, e_s^{Δ}) point of Fig. A1. The intersection point of the line tangent $\Delta(T_a)$ [i.e., $e = \Delta(T_a)(T - T_a) + e^*(T_a)$] and the E_p line of $e = (T - T_a)\,(e_{ws}^{SJ} - e_a)/(T_{ws} - T_a) + e_a$ is obtained by their mutual solution of the T and e values as

$$T_s^{\Delta} = T_a + \frac{e^*(T_a) - e_a}{\frac{e_{ws}^{SJ} - e_a}{T_{ws}^{SJ} - T_a} - \Delta(T_a)} \tag{A1}$$

$$e_s^{\Delta} = \Delta(T_a)\left(T_s^{\Delta} - T_a\right) + e^*(T_a) \tag{A2}$$

The surface isenthalp going through this point intersects the saturation vapor pressure curve at T_{ws}^{Q} (Fig. A1), obtainable by the same iteration process employed in Eq. (6) but with T_s^{Δ}, e_s^{Δ}.

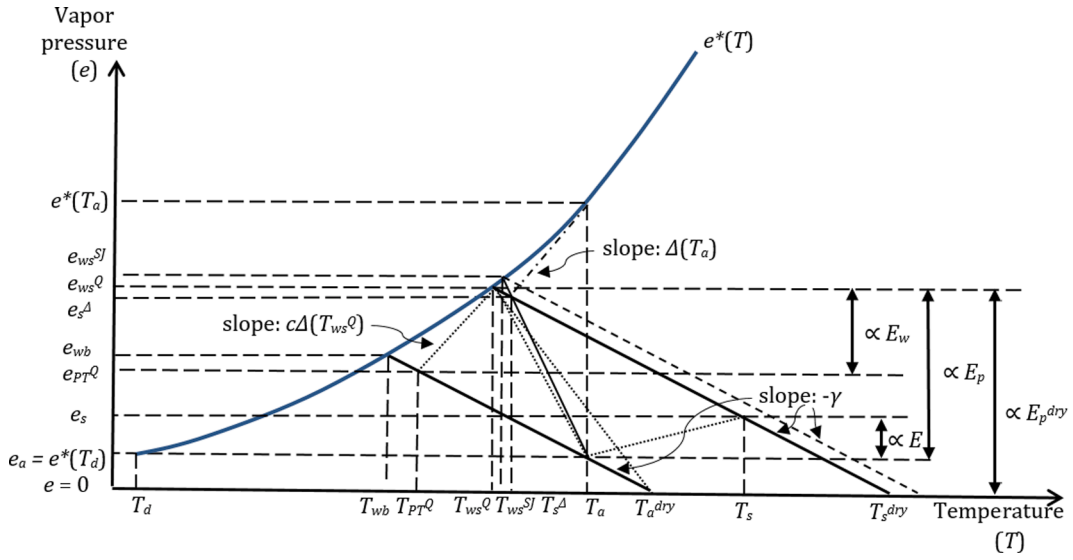

Fig. A1. Same as Fig. 1, but Qualls and Crago (2020) shifts the surface isenthalp to the left of its position from Fig. 1. See Table 1 for the definition of additional temperature and evaporation terms, and the text for explanation.

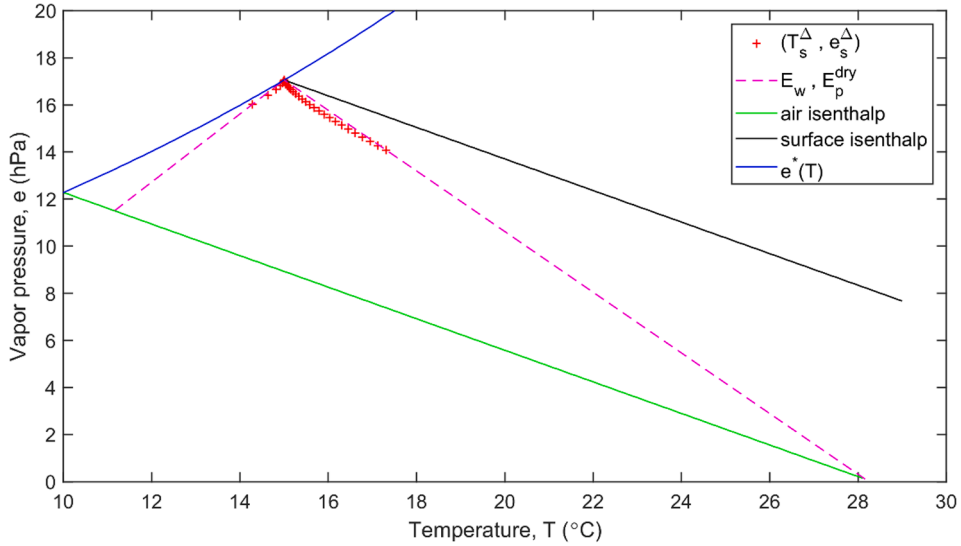

Fig. A2. Successive sample locations of the intersection of the E_p line of Figs. 1 & A1, and the line tangent $\Delta(T_a)$ (not displayed here for clarity) during complete dry out of the environment. The E_p line rotates around [T_{ws}, $e^*(T_{ws})$] between the two limit lines of E_w [left intermittent line, yielding (T_{PT}, e_{PT}) at its intersection with the air isenthalp] and E_p^{dry}, displayed. Prescribed values: $T_{wb} = 10$ °C, $T_{ws} = 15$ °C, $\alpha = 1.1$.

This intersection point however progressively climbs upward on the phase diagram (Fig. A2) before T_a reaches T_{ws}^{SJ} from its starting value of T_{PT}^{Q} during adiabatic drying out of the environment from a fully wet condition. At $T_a = T_{ws}^{SJ}$, the intersection point is on the saturation vapor pressure curve, yielding T_{ws}^{SJ}. With additional drying of the environment the intersection point starts to fall (Fig. A2) as the (T_a, e_a) point slides further down the air isenthalp and simultaneously [T_a, $e^*(T_a)$] climbs higher on the saturation vapor pressure curve. The corresponding surface isenthalps that should go through these temporally changing intersection points, parallel with the unchanging one going through (T_{ws}^{SJ}, e_{ws}^{SJ}), would also yield temporally changing wet surface temperatures (i.e., T_{ws}^{Q} in Fig. A1), which is a physical contradiction, as the value of T_{ws} is strictly tied to that of T_{wb} by a constant Q_n and wind speed, as was pointed out by Monteith (1981) and experimentally proven by Szilagyi (2014) (see Appendix II for the latter).

As seen, the T_{ws} correction of Qualls and Crago (2020) pushes the surface isenthalp closer to the air one, thus depressing the $e_s - e_a$ difference, and so the estimated actual evaporation value. As it leads to physical contradictions, it is not tested further.

Appendix II

Empirical proof of the wet-surface temperature invariability during near-isenthalpic environmental conditions. In the months of July between 2000 and 2009, 0.7° ERA-Interim grid cells (https://www.ecmwf.int/en/forecasts/datasets/reanalysis-datasets/era-interim) with the same (up to a ± 2% difference) monthly Q_n values were selected from Central Nebraska, USA, together with PRISM-calculated (Daly et al., 1994) and ERA-Interim cell-averaged monthly T_a and T_d values (prism.oregonstate.edu) (Fig. A3). The Q_n, T_a, and T_d values were then plotted against the mean monthly MODIS-derived daytime surface temperatures (T_{s_dt}, from https://lpdaac.usgs.gov/lpdaac/products/modis_ products_table) as a proxy for the wetness index, w, (the lower the T_{s_dt} value the wetter the area), averaged also over the same 0.7° grid cells. Central Nebraska, due to its vast irrigated areas adjacent to the non-irrigated and relatively dry Sand Hills region, provides an ideal test-ground for obtaining a wide range of wetness conditions under the same Q_n.

Note the quasi-horizontal, near-parallel, sum-of-squares fitted lines for T_{wb} of Eq. (6) and T_{ws} of Eq. (8), experimentally proving that not only T_{wb} but T_{ws} as well stay constant under isenthalpic wetting/drying cycles of the environment.

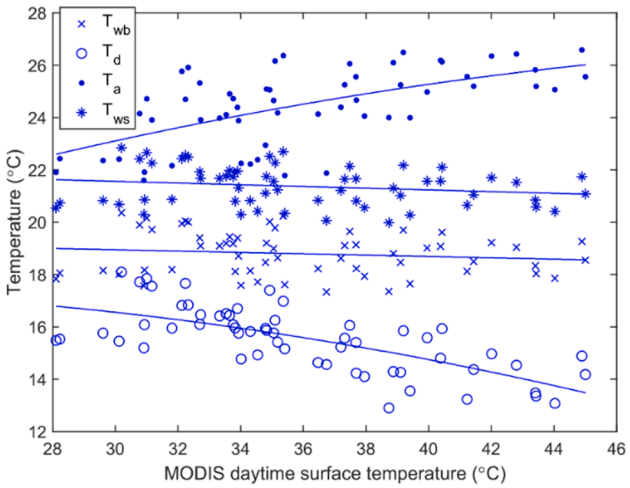

Fig. A3. PRISM-derived mean daily T_a and T_d values in July (2000–2009) as a function of MODIS-derived daytime surface temperature, both aggregated to the 0.7° ERA-Interim cells of central Nebraska, USA, having $Q_n = 143 \pm 2.86$ W m^{-2} to ensure a spatially quasi-constant energy available at the surface. The straight lines are the near-constant best fitting first-, while the curves, second-order polynomials. The sample mean (size of 59) with the corresponding standard deviation value for T_{wb} is 18.8 ± 0.82, and for T_{ws} it is 21.37 ± 0.76 °C (after Szilagyi, 2014).

References

Aminzadeh, M., Roderick, M.L., Or, D., 2016. A generalized complementary relationship between actual and potential evaporation defined by a reference surface temperature. Water Resour. Res. 52 (1), 385–406. https://doi.org/10.1002/2015WR017969.

Bouchet, R.J., 1963. Evapotranspiration réelle et potentielle, signification climatique. IAHS Publ. 62, 134–142.

Brutsaert, W. (Ed.), 1982. Evaporation into the Atmosphere. Springer Netherlands, Dordrecht.

Brutsaert, W., 2015. A generalized complementary principle with physical constraints for land-surface evaporation. Water Resour. Res. 51 (10), 8087–8093. https://doi.org/10.1002/2015WR017720.

Brutsaert, W., Li, W., Takahashi, A., Hiyama, T., Zhang, L.u., Liu, W., 2017. Nonlinear advection-aridity method for landscape evaporation and its application during the growing season in the southern Loess Plateau of the Yellow River basin: Landscape evaporation. Water Resour. Res. 53 (1), 270–282. https://doi.org/10.1002/2016WR019472.

Brutsaert, W., Cheng, L., Zhang, L., 2020. Spatial distribution of global landscape evaporation in the early twenty first century by means of a generalized complementary approach. J. Hydromet. 21, 287–298. https://doi.org/10.1175/JHM-D-19-0208.1.

Crago, R., Szilagyi, J., Qualls, R., Huntington, J., 2016. Rescaling the complementary relationship for land surface evaporation: Rescaling the complementary relationship. Water Resour. Res. 52 (11), 8461–8471. https://doi.org/10.1002/2016WR019753.

Crago, R.D., Qualls, R.J., 2018. Evaluation of the generalized and rescaled complementary evaporation relationships. Water Resour. Res. 54 (10), 8086–8102. https://doi.org/10.1029/2018WR023401.

Daly, C., Neilson, R.P., Phillips, D.L., 1994. A statistical-topographic model for mapping climatological precipitation over mountainous terrain. J. Appl. Meteor. 33 (2), 140–158. https://doi.org/10.1175/1520-0450(1994)033<0140:ASTMFM>2.0.CO;2.

Han, S., Hu, H., Tian, F., 2012. A nonlinear function approach for the normalized complementary relationship evaporation model: Nonlinear function approach for complementary relationship model. Hydrol. Process. 26 (26), 3973–3981. https://doi.org/10.1002/hyp.8414.

Han, S., Tian, F., 2018. Derivation of a sigmoid generalized complementary function for evaporation with physical constraints. Water Resour. Res. 54 (7), 5050–5068. https://doi.org/10.1029/2017WR021755.

Han, S., Tian, F., 2020. A review of the complementary principle of evaporation: from the original linear relationship to generalized nonlinear functions. Hydrol. Earth Syst. Sci. 24, 2269–2285. https://doi.org/10.5194/hess-24-2269-2020.

LHOMME, J.-P., 1997. A theoretical basis for the Priestley-Taylor coefficient. Boundary Layer Meteorol. 82 (2), 179–191. https://doi.org/10.1023/A:1000281114105.

Ma, N., Szilagyi, J., 2019. The CR of evaporation: A calibration-free diagnostic and benchmarking tool for large-scale terrestrial evapotranspiration modeling. Water Resour. Res. 55 (8), 7246–7274. https://doi.org/10.1029/2019WR024867.

Ma, N., Szilagyi, J., Zhang, Y., Liu, W., 2019. Complementary-relationship-based modeling of terrestrial evapotranspiration across china during 1982–2012: Validations and spatiotemporal analyses. J. Geophys. Res. Atmos. 124 (8), 4326–4351. https://doi.org/10.1029/2018JD029850.

Ma, N., Szilagyi, J., Zhang, Y., Jozsa, J., 2020. Benchmarking large-scale evapotranspiration (ET) estimates: A perspective from a calibration-free complementary relationship (CR) approach and FLUXCOM. J. Hydrol. 125221 https://doi.org/10.1016/j.jhydrol.2020.125221.

Mamtimin, A., Wang, Y., Sayit, H., Yang, X.H., Yang, F., Huo, W., Zhou, C., 2020. Seasonal variations of the near-surface atmospheric boundary layer structure in China's Gurbantunggut Desert. Adv. Meteor. 2020, 6137237. https://doi.org/10.1155/2020/6137237.

McNaughton, K.G., Spriggs, T.W., 1989. An evaluation of the Priestley-Taylor equation and the complementary relationship using results from a mixed-layer model of the convective boundary layer. IAHS Publ. 177.

Monteith, J.L., 1981. Evaporation and surface temperature: Evaporation and surface temperature. Q.J.R. Meteorol. Soc. 107 (451), 1–27. https://doi.org/10.1002/qj.49710745102.

Morton, F.I., 1983. Operational estimates of areal evapotranspiration and their significance to the science and practice of hydrology. J. Hydrol. 66 (1–4), 1–76. https://doi.org/10.1016/0022-1694(83)90177-4.

Penman, H.L., 1948. Natural evaporation from open water, bare soil and grass. Proc. Royal Soc. A Math Phys. Eng. Sci. 193, 120–145. https://doi.org/10.1098/rspa.1948.0037.

PRIESTLEY, C.H.B., TAYLOR, R.J., 1972. On the assessment of surface heat flux and evaporation using large-scale parameters. Mon. Wea. Rev. 100 (2), 81–92. https://doi.org/10.1175/1520-0493(1972)100<0081:OTAOSH>2.3.CO;2.

Qualls, R.J., Crago, R.D., 2020. Graphical interpretation of wet surface evaporation. Water Resour. Res. https://doi.org/10.1029/2019WR026766.

Shuttleworth, W.J., Serrat-Capdevila, A., Roderick, M.L., Scott, R.L., 2009. On the theory relating changes in area-average and pan evaporation. Quart. J. Royal Meteor. Soc. 135, 1230–1247. https://doi.org/10.1002/qj.

Stull, R.B., 2000. Meteorology for Scientists and Engineers. Brooks/Cole, Pacific Grove, CA, USA.

Szilagyi, J., 2014. Temperature corrections in the Priestley–Taylor equation of evaporation. J. Hydrol. 519, 455–464. https://doi.org/10.1016/j.jhydrol.2014.07.040.

Szilagyi, J., Schepers, A., 2014. Coupled heat and vapor transport: The thermostat effect of a freely evaporating land surface: Szilagyi et al.: Coupled heat/vapor transport. Geophys. Res. Lett. 41 (2), 435–441. https://doi.org/10.1002/2013GL058979.

Szilagyi, J., 2018. A calibration-free, robust estimation of monthly land surface evapotranspiration rates for continental-scale hydrology. Hydrol. Res. 49 (3), 648–657. https://doi.org/10.2166/nh.2017.078.

Szilagyi, J., Jozsa, J., 2008. New findings about the complementary relationship-based evaporation estimation methods. J. Hydrol. 354 (1-4), 171–186. https://doi.org/10.1016/j.jhydrol.2008.03.008.

Szilagyi, J., Crago, R., Qualls, R., 2017. A calibration-free formulation of the complementary relationship of evaporation for continental-scale hydrology: Calibration-free CR. J. Geophys. Res. Atmos. 122 (1), 264–278. https://doi.org/10.1002/2016JD025611.

Szilagyi, J., Crago, R., Ma, N., 2020. Dynamic scaling of the generalized complementary relationship (GCR) improves long-term tendency estimates in land evaporation. Adv. Atmos. Sci. 37 (9), 1–12. https://doi.org/10.1007/s00376-020-0079-6.

Update

Journal of Hydrology

Volume 595, Issue , April 2021, Page

DOI: https://doi.org/10.1016/j.jhydrol.2021.126031

Journal of Hydrology 595 (2021) 126031

Contents lists available at ScienceDirect

Journal of Hydrology

journal homepage: www.elsevier.com/locate/jhydrol

Corrigendum to "On the thermodynamic foundations of the complementary relationship of evaporation" [J. Hydrol. (2021) 125916]

Jozsef Szilagyi [a,b]

[a] Department of Hydraulic and Water Resources Engineering, Budapest University of Technology and Economics, H-1111 Muegyetem Rkp. 1-3, Budapest, Hungary
[b] Conservation and Survey Division, School of Natural Resources, University of Nebraska-Lincoln, Lincoln, Nebraska, USA

With the application of the differentiation rule of ratios and consideration to $e_a = e_s = 0$ at $w = 0$, the relative changes (dy vs dX) in y and X of Eqs. (19) and (20) at $w = 0$ are as follows: $dy = d(E/E_p) = (de_s - de_a)/E_p$ and $dX = d[(e_a E_w)/(e_{PT} E_p)] = E_w/e_{PT}\, d(e_a/E_p) = E_w/e_{PT}\, de_a/E_p$, yielding the same result as published, i.e., $dy/dX = [(de_s - de_a)/de_a]e_{PT}/E_w$. The original text is correct if in the paragraph above Eq. (26) the 'd' in 'dE_p' terms is deleted.

The error is deeply regretted by this author.

DOI of original article: https://doi.org/10.1016/j.jhydrol.2020.125916.
E-mail address: szilagyi.jozsef@epito.bme.hu.

https://doi.org/10.1016/j.jhydrol.2021.126031

Available online 2 February 2021